



Nanoscale

Pediatric glioblastoma target-specific efficient delivery of gemcitabine across blood-brain barrier via carbon nitride dots

Journal:	<i>Nanoscale</i>
Manuscript ID	NR-ART-02-2020-001647
Article Type:	Paper
Date Submitted by the Author:	26-Feb-2020
Complete List of Authors:	Liyanage, Piumi; University of Miami Zhou, Yiqun; University of Miami, Chemistry Alyoubi, Abdulrahman; King Abdulaziz, Chemistry Bashammakh, A; King Abdulaziz U, El-Shahawi, Mohammad; King Abduazaz U, Chemistry Vanni, Steven; University of Miami Miller School of Medicine, Neurological Surgery Graham, Regina; University of Miami School of Medicine, Department of Neurological Surgery Leblanc, Roger; University of Miami, Department of Chemistry

SCHOLARONE™
Manuscripts

Pediatric glioblastoma target-specific efficient delivery of gemcitabine across blood-brain barrier via carbon nitride dots

Piumi Y. Liyanage ¹, Yiqun Zhou ¹, Abdulrahman O. Al-Youbi ², Abdulaziz S. Bashammakh ², Mohammad S. El-Shahawi ², Steven Vanni ³, Regina M. Graham ^{3,4}, Roger M. Leblanc ^{1,*}

¹Department of Chemistry, University of Miami, Coral Gables, FL 33146, USA.

²Department of Chemistry, King Abdulaziz University, P.O. Box 80200, Jeddah 21589, Kingdom of Saudi Arabia.

³Department of Neurological Surgery, Miller School of Medicine, University of Miami, Miami, Florida 33136, USA.

⁴Sylvester Comprehensive Cancer Center, University of Miami Miller School of Medicine, 1475 NW 12th Ave, Miami, Florida 33136, USA.

*Corresponding Author.

E-mail Address: rml@miami.edu

ABSTRACT

Pediatric glioblastomas are known to be one of the most dangerous and life-threatening cancers among many other regardless of the low number of cases reported. The major obstacles in the treatment of this tumor can be identified as the lack of prognosis data and the therapeutic requirement to be able to cross the blood-brain barrier (BBB). Due to this lack of data and techniques, pediatric patients could face drastic side effects over a long-time span even after survival. Therefore, in this study, the capability of non-toxic carbon nitride dots (CNDs) to selectively target pediatric glioblastoma cells was studied *in vitro*. Further, the nanocarrier capability and efficiency of CNDs was also investigated through conjugation of a chemotherapeutic agent and transferrin (T_f) protein. Gemcitabine (GM) was introduced to the system as the chemotherapeutic agent, which has never been successfully used for the treatment of any central nerves system (CNS) cancer. More than 95% of selective damaging of SJGBM2 glioma cells was observed at 1 μ M of CN-GM conjugate with almost 100% viability of non-cancerous HEK293 cells, although this ability was diminished at lower concentrations. However, by further conjugation of T_f to obtain CN-GM- T_f , allowed the achievement of selective targeting and prominent anti-cancer activity at a 100-fold lower concentration at 10 nM. Furthermore, both conjugates were capable of effectively damaging several other brain tumor cells, which were not well responsive towards the single treatment of GM. The capability of BBB penetration of the conjugates was observed using a zebrafish model, which confirms the CNDs' competence as an excellent nanocarrier to CNS.

1. Introduction

Cancer has been one of the highest fatality rate diseases for the last few decades in the world, regardless of being one of the most researched in medicinal and scientific fields. Among the various types of cancers, brain tumors can be identified as one of the most dangerous given its location, the difficulty of treatment and recurrence possibility.¹ Thus, with the current treatment techniques the disease remains with very low survival rate beyond 5-years. This abnormal cell growth in the brain is categorized into two types, primary and secondary, whereas primary being the tumors that arise in the brain as benign or malignant while secondary brain tumors being the metastasis of cancers into the brain from elsewhere in the body. The most common cancers that can metastasize into the brain are lung and breast cancers, where about half of it is due to lung cancers.² Due to its location enclosed inside the brain skull, the uncontrolled growing mass of the tumor can also compress, dislocate normal brain tissues and block the flow of cerebrospinal fluid (CSF). Brain tumors are generally categorized according to their area of origin in the brain and the rate of growth of the tumor cells. Among these, gliomas are referred to as one of the most commonly reported central nervous system (CNS) tumors of all ages.³ Arising from the glial cells hence the name, gliomas are categorized as low-grade gliomas (I and II) and high-grade gliomas (III and IV). In children from age 0-18 years, the low-grade gliomas predominate whereas in adults the high-grade gliomas are prominent. Regardless, the pediatric high-grade gliomas have shown to be aggressive with less biological data available for prognosis.⁴ Mostly the pediatric clinical treatments have been relied on similar adult trial data and have also gained similar outcomes.^{5,6} However, recent studies have shown that the pediatric gliomas have different genomic and biological complexities from their adult versions.^{7,8} Thus, even though the reported 5-year survival rate of pediatric brain tumor patients is higher than that of the adult counterparts, poor prognosis can still cause unknown problems in pediatric brain tumor treatments. Furthermore, a major hurdle in pediatric tumor treatment is the severe adverse side effects incurred due to the drugs. Many of the treatments include chemotherapeutic agents that showed positive results in adult clinical trials, such as doxorubicin,⁹ temozolomide¹⁰ and vemurafenib.¹¹ But, all these agents are non-targeting therapeutics and thus, tend to damage healthy cells and tissues in the surrounding area and even elsewhere in the body.^{12,13} When used on pediatric patients whose organs are still developing, these can cause drastic, long-lasting and even life-threatening side effects.¹⁴⁻¹⁶ Therefore, selective targeting of suitable regimens is critically important in pediatric tumor treatments.

Successful treatment of any cancer relies on the ability to deliver therapeutic regimens to the tumor sites in pharmacologically effective doses. In the case of brain tumors, the inability of many drugs to penetrate the blood-brain barrier (BBB) to enter the central nervous system has hindered the success of many treatments and research.¹⁷ It is well known that BBB hinders any unwanted molecules crossing into the CNS to avoid any possible harmful effects or toxicities. But this biological barrier also acts as a large therapeutic obstacle only allowing certain molecules with specific characteristics to pass through.¹⁸ Thus, several researches have been

conducted so far to detect possible techniques or payload carriers to cross the BBB to help enhance the treatment deficiencies of CNS based diseases. Few techniques that have been reported so far use force to break out a small junction through the endothelial cells by heat treatments, ultra sounds, osmotic pressure and microbubbles which involve high risks.¹⁹⁻²¹ Later, rather than disrupting the barrier, many studies were involved in using nanoparticles to cross the BBB for imaging and drug delivery.^{22,23} Moreover, using proteins such as transferrin (T_f) as a Trojan horse molecule to overcome the barrier through receptor-mediated endocytosis also became popular.²⁴ T_f is a large protein with an approximate molecular weight of 80 kDa and it is mainly responsible for the iron circulation in the cells. Studies have found that T_f receptors are abundant in certain cells according to their needs and BBB also consists of a fair amount of T_f receptors due to the iron transporter needs of the brain. It has also been previously reported that many cancer cells contain abundant of T_f receptors on the cell membrane due to their high metabolic requirements.²⁵ Thus, T_f has also become a targeting molecule in tumor treatments. Soe *et al.* reported a study of T_f conjugated system on a polymeric nanoparticle for targeted chemotherapeutic delivery of doxorubicin into resistant breast cancer cells with lower toxicity towards healthy cells.²⁶

Gemcitabine (GM) is an anti-cancer therapeutic used for several types of cancer treatments such as pancreatic, bladder, ovarian and breast. GM is a potent inducer of cancer cell death. The mechanism of activity of this in the cells is to block the DNA polymerase activity, thus inhibiting further DNA synthesis and inducing cell death.²⁷ Upon uptake into the cells GM metabolites into its active forms of gemcitabine triphosphate and gemcitabine diphosphate prior to the DNA attack.²⁸ In addition, GM is a strong radiosensitizer and acts synergistically with a number of chemotherapeutic agents. In regard to brain tumors, GM is an attractive agent and preclinical studies demonstrate potent anti-glioma effects. However, clinical trials examining the potential of GM for the treatment of adult GBM have been largely disappointing.²⁹⁻³¹ Similarly, a recent clinical trial combined GM and radiotherapy was examined in newly diagnosed children with high-grade glioma found no increase in overall survival.³² This could be attributed to short plasma half-life, poor BBB penetration and dose-limiting toxicities.^{31,33,34} Therefore, efforts are underway to increase GM delivery across the BBB to brain tumors at therapeutic levels.

Carbon nitride dots (CNDs), a sub class of carbon dots is a novel nanocarrier material. Similar to carbon dots, its unique characteristics such as nano size, good water dispersibility, high photoluminescence (PL), non-toxicity and good biocompatibility allows their use in biological and medical approaches.^{35,36} Due to the excitation-dependent PL emission and high quantum yields, these dots are immensely popular in bioimaging studies. Further, CNDs structure can be manipulated according to the synthesis methodology being used. Thus, these nanoparticles can be specifically used in different applications depending on their unique structural characteristics.³⁷⁻³⁹ In this study, the CNDs we synthesized were found to have carboxylic functional groups on the surface which we utilized in the conjugation to obtain our desired products.⁴⁰ Furthermore, these CNDs were found to contain amine and amide functional groups

on the surface apart from the carboxylic groups which together could enable its selective entry into pediatric cancer cells.

Overall, this study aims at 1) the synthesis of conjugates containing GM and/or T_f on to the CNDs, 2) the capability of using this nanocarrier system for the selective targeting of the high-grade pediatric glioblastoma cells without affecting non-cancer cells, 3) the capability of this nanosystem to cross the BBB to enter the CNS, 4) enhance the drug efficacy compared to single treatment of drug.

2. Experimental

Materials

Anhydrous citric acid (BDH) was obtained from VWR (West Chester, PA). Urea was acquired from Eastman Kodak Company (NY, USA). Holo-transferrin (human plasma) was from EMD Millipore Corp., (MA, USA). N-Hydroxysuccinimide (NHS), 1-ethyl-3-(3-dimethylaminopropyl) carbodiimide (EDC) and gemcitabine hydrochloride were purchased from Millipore-Sigma (St. Louis, MO). Two types of dialysis tubing were used. The tubing with 1000 Da molecular weight cut-off was obtained from Spectrum Labs Inc., (CA, USA) while the 3500 Da molecular weight cut-off tubing was from Thermo-Scientific (Rockford, IL). The deionized (DI) water used was ultrapure (type I) water purified using a Millipore Direct-Q 3 water purification system acquired from EMD Millipore Corp. The purified water has a surface tension of 72.6 mN·m⁻¹, a resistivity of 18 MΩ·cm and a pH of 6.6 ± 0.3 at 20.0 ± 0.5 °C. All the chemicals were used as received.

Synthesis of the Carbon-Nitride Dots (CN Dots)

The CNDs were synthesized using the same process described in our previous report using citric acid and urea. The characterization of the CNDs was performed to confirm the reproducibility and the same results were obtained as reported.⁴⁰

Synthesis of the CN Dots – gemcitabine conjugate (CN-GM)

The synthesized CNDs (8 mg) were dissolved in 3 ml of phosphate buffered solution (PBS, pH 7.4 at 25 mM). 1-ethyl-3-(3-dimethylaminopropyl) carbodiimide (EDC, 17 mg in 1 ml PBS) was also added to the same flask containing CNDs and was stirred at room temperature for 30 min. Then, a solution of 1 ml PBS containing 10.2 mg of N-hydroxysuccinimide (NHS) was added to the above same reaction mixture. After another 30 min. of stirring, the gemcitabine hydrochloride solution (GM, 5 mg in 1 ml PBS) was mixed with the reaction mixture and was left stirring for overnight. Then the solution was transferred into 1 kDa molecular weight cut-off dialysis tubing and was dialyzed against 2 L of DI water for 4 days with water changing every 24 h. Finally, the remaining solution was freeze-dried to yield the lyophilized powder.

Synthesis of the CN Dots – gemcitabine - transferrin conjugate (CN-GM-T_f)

The CNDs (8 mg in 3 ml PBS) was mixed with EDC (17 mg in 1 ml PBS) and was stirred at room temperature for 30 min. Then, a solution of 1 ml PBS containing 10.2 mg of NHS was added to the same reaction mixture. After another 30 min. of stirring, the GM, (5 mg in 1 ml PBS) was added and left stirring for another 30 min. Then a solution of 1 ml PBS containing transferrin (1 mg) was slowly added to the reaction mixture and was left stirring for overnight before stopping the reaction. Then the solution was transferred into 3.5 kDa molecular weight cut-off dialysis tubing and was dialyzed against 2 L of DI water for 4 days with water changing every 24 h. Finally, the remaining solution was freeze-dried to yield the lyophilized powder.

Characterization of the CN Dots – gemcitabine conjugate and CN Dots – gemcitabine - transferrin conjugate

The as-prepared CN-GM and CN-GM-T_f conjugates were characterized by UV-Vis absorption using a Cary 100 UV-Vis spectrophotometer (Agilent Technologies) in aqueous medium in a 1 cm quartz cuvette (Starna Cells). A Horiba Jobin Yvon Fluorolog-3 spectrometer was used to observe the luminescent emission (in 1 cm path length quartz cuvette) using a slit width of 5 nm for both excitation and emission. OriginPro 9.1 was used to create the normalization of the emission spectra. The normalization was performed with the y-axis normalized to 1. The Fourier transform infrared (FTIR) spectra were recorded in a PerkinElmer Frontier with a universal ATR sampling accessory using air as the background. The samples were also analyzed through mass spectroscopy using matrix-assisted laser desorption ionization time of flight (MALDI-TOF) (Bruker). Zeta potential measurements and DLS size measurements were carried out with the use of a DLS nano series Malvern Zetasizer. Further, transmission electron microscopy (TEM) was performed using a JEOL 1200X TEM.

Cell culture and cell viability studies with MTS assay

Pediatric GBM (SJGBM2, CHLA200) and CHLA266 (Atypical teratoid rhabdoid tumor, AT/RT) cell lines were obtained from Children's Oncology Group (COG, Lubbock, TX) and U87 (adult GBM cell line), HEK293 (human embryonic kidney cell line) were from American Type Culture Collection (ATCC, Manassas, VA, USA). RPMI-1640 media (ThermoFisher Scientific, Waltham, MA, USA) was used as the cell culture media, supplemented with heat inactivated 10% fetal bovine serum (FBS) and 1% penicillin/streptomycin (both from Gemini Biosciences, West Sacramento, CA) and maintained by incubating at 37 °C in humidified 5% CO₂. Routine testing was conducted for mycoplasma using LookOut mycoplasma PCR detection kit (Sigma Aldrich, St. Louis, MO) on all cell lines according to the manufacturer's instructions.

Cell viability was determined using CellTiter 96[®] AQueous One Solution Cell Proliferation Assay (MTS) (Promega Madison, WI). 96-well plates were used for cell plating at a density of 0.5-2 x 10⁴ cells per well in 100 µL of cell culture media and incubated for 24 h. At the end of 24 h, cells were treated with a series of concentration of single agent GM, CN-GM and CN-GM-T_f

ranging from 10 μM – 1 nM, dispersed in 100 μL RPMI. Cell viability determination with MTS assay was conducted after 72 h of incubation as per manufacturer instructions. For viability measurements absorbances were recorded at 490 nm using BoiTek Synergy HT plate reader.

In vitro bioimaging

FBS coated glass coverslips were placed in a 24-well plate. Then, SJGBM2 and HEK293 cells were plated on the coverslips at a density of 1×10^4 in 200 μL RPMI and incubated for 24 h for sufficient cell growth. The media was aspirated out and cells were retreated with 200 μL RPMI solutions containing 50 $\mu\text{g}/\text{ml}$ of CN-GM and CN-GM- T_f conjugates and further incubated for 24 h. Cells were washed with PBS and fixed with 4% paraformaldehyde for 20 min. The coverslips were mounted on to glass slides before imaging on an Olympus FV1000 confocal microscope and an Olympus BX51 inverted fluorescence microscope. Fluorescence intensity quantification measurements were obtained using imageJ and the statistical analysis were performed using jmp pro15.

Zebrafish injection and bioimaging

Wild-type zebrafish larvae 5 days post fertilization (dpf) were provided by the Zebrafish Core Facility at University of Miami. 10 mg/mL naked CNDs or CN-GM conjugate aqueous dispersion was intravascularly (IV) injected into the heart of the zebrafish that had been anesthetized in 30 mL buffered embryo media which contained 2 mL 0.4% tricaine solution. After 5 min, the injected zebrafish (number: 12) were mounted with low-melting agar on a round quartz plate for observation under the Leica SP5 confocal microscope under white light and excitation at 405 nm (for both naked CNDs and CN-GM conjugate). The animal care protocol for all procedures used in this study was approved by the University of Miami Animal Care and Use Committee and complies with the guidelines of the National Science Foundation.

3. Results and Discussion

The CNDs were prepared using the same synthesis technique mentioned in our previous publication, with citric acid and urea as the precursors.⁴⁰ The performed characterizations confirmed that the yielded product is the same CNDs as reported by us previously.

Conjugate synthesis and characterization

The drug and protein loading on to the CNDs was achieved by forming carbodiimide crosslinking between the CNDs and the loading molecules. A traditional EDC / NHS bioconjugation approach was used. The carboxyl functionalities on the surface of the CNDs are activated by EDC for a direct reaction with the primary amine functional groups present on the loading molecules. The crosslinking was conducted at neutral pH (7.4) in phosphate buffer

(PBS) which lowers the actual activation efficiency of EDC. Thus, the molar ratio of CND to EDC was kept at 1:8 to compensate the reduced efficiency. To prevent hydrolysis of the fairly unstable O-acylisourea intermediate formed through EDC crosslinking, NHS was also included in the coupling reaction to further form a considerably more stable ester which then allows efficient zero-length coupling with primary amines by forming a peptide bond. Thus, both the chemo drug, GM and the receptor protein, T_f can be effectively loaded with high loading capacity on to the nanocarrier, CNDs through covalent conjugation. The molar ratio of GM : CNDs was kept at 2:1 for the synthesis of CNDs-gemcitabine conjugate (CN-GM) as well as CNDs-gemcitabine-transferrin conjugate (CN-GM- T_f). Since, T_f is a significantly larger molecule compared to CND and GM, it was kept as the limiting reagent in the synthesis procedure of CN-GM- T_f , so as to minimize the burden in purifying procedure. Thus, the working precursor molar ratio was used as 1 : 2 : 0.001 for CND : GM : T_f respectively. The final synthesis mixture was dialyzed against DI water to remove any small and unconjugated molecules. Then the conjugated products, CN-GM and CN-GM- T_f were freeze dried to yield their powder forms. The conjugates were studied using UV-Vis absorption, fluorescence and MALDI-TOF mass spectrometry to confirm the conjugation.

GM was found to have an absorption band at around 325 nm (Fig. 1), which could be arising from the C=O functional present in its structure. This band overlaps the absorption of naked CNDs, which has absorption bands at around 345 and 400 nm. Thus, it is possible that the high intensity absorption of CND bands has overwhelmed the presence of the comparatively weak GM band in the conjugates. Furthermore, the pure T_f shows an absorption band at 280 nm, owing to the tryptophan present in its protein structure. But this band also is not clearly visible in the obtained absorption spectrum of CN-GM- T_f conjugate shown in Fig. 1. This could also be due to the low quantity of transferrin contained in the conjugate comparatively, thus containing less tryptophan which is solely responsible for the absorption band. Other than this, the fact that the said band overlaps the overwhelming absorption region of CNDs between 200 to 400 nm is also a drawback.

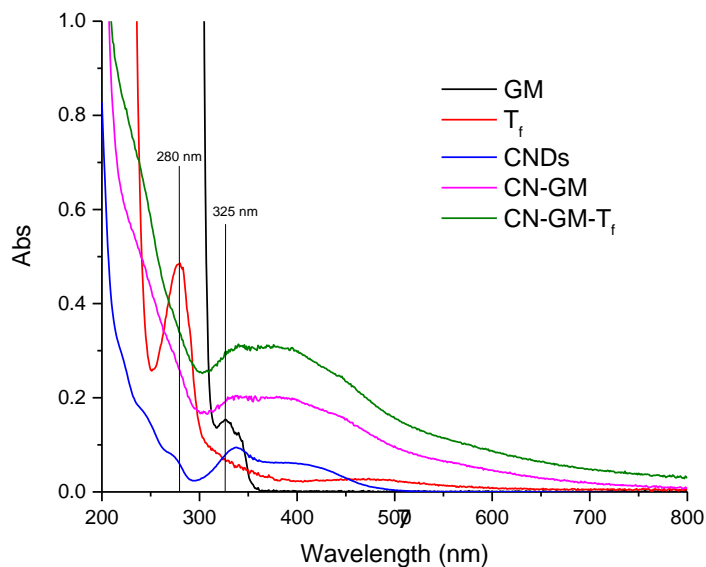


Fig. 1 UV-Vis absorption spectra of pure GM (black), pure T_f (red), CNDs (blue), CN-GM conjugate (purple), CN-GM-T_f conjugate (green).

For further optical property investigations, PL of the conjugates were studied. Since all three components (CNDs, GM, T_f) separately show luminescence, it was compared to the luminescence of the two conjugates. The observed PL spectra for each conjugate (Fig. 2A for CN-GM and Fig. 2B for CN-GM-T_f) shows the excitation-dependent PL emission characteristic for the CNDs which is consistent with our previous publication and also corresponds to typical behavior for many of such carbon-based nanomaterials (carbon dots).^{41,42} Further, both conjugates show the CNDs emission at 450 nm when excited at 370 nm. But the maximum PL emission for both conjugates has red shifted by about 20 nm from the previously recognized maximum CNDs emission wavelength confirming the presence of the conjugate. Furthermore, this is visible in the excitation spectra in the region of 300-350 nm, which clearly show two distinguished bands in the emission for both conjugates. Although GM is capable of showing PL, the high intensity spectra of CNDs overwhelm the presence of the weak PL of GM (Fig. 2C). GM alone shows an emission band at around 390 nm when excited at its highest absorption, 325 nm although the spectra illustrate small shifts when the excitation wavelength is changed which could occur due to its structure containing aromatic rings. At lower excitation wavelengths the conjugates show comparatively lower emission intensities, possibly due to the high inner absorption of the solution without light emission. Therefore, the tryptophan PL emission from T_f at 345 nm when excited at 280 nm is almost non-existent in the conjugate, CN-GM-T_f. The limiting amount of T_f present is also a factor responsible for the reduced emission observed.

To understand the conjugation in relevance to surface structural functional groups, FTIR spectra of both conjugates in solid state were obtained using an ATR accessory (Fig. 3). Both conjugates showed subtle differences in comparison to the naked CNDs. Both CN-GM (red) and CN-GM-T_f (blue) have a more intense band at around 3315 cm⁻¹ compared to naked CNDs which can be attributed to amide N-H stretching, while the carboxylic O-H stretch⁴³ present at around 2790 cm⁻¹ in the naked CNDs is not prominent in the spectra of the conjugates. Moreover, the band at 1710 cm⁻¹ shown in the spectrum of CNDs resulting from carboxylic C=O stretching has become less notable in the spectra of the conjugates whereas the 1630 cm⁻¹ band corresponding to amide I band has become stronger. Therefore, these changes confirm the availability of abundant peptide bonds confirming the presence of the conjugates which were synthesized through formation of peptide bonds between the three compounds using the carboxylic and amine groups present on them.

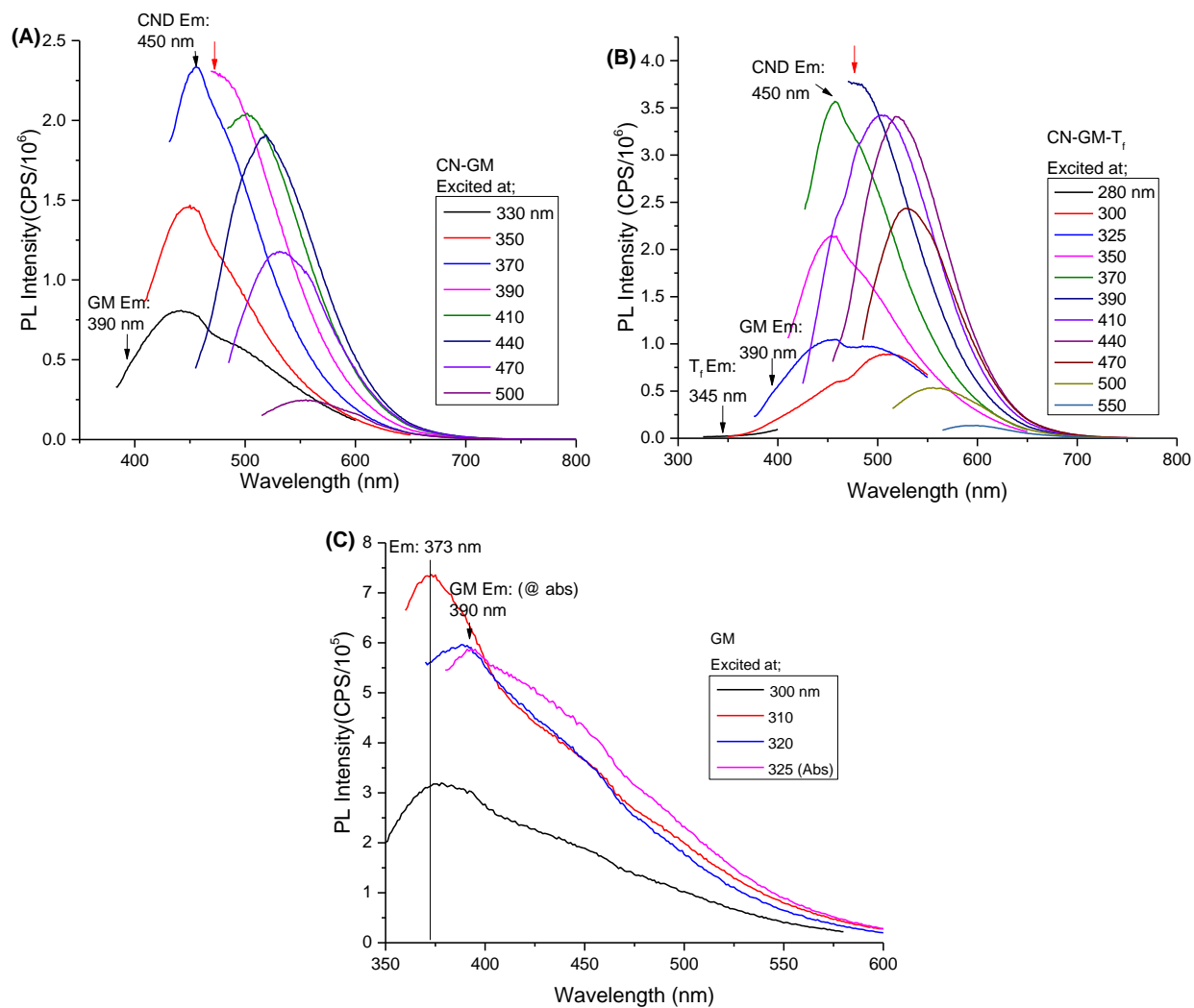


Fig. 2
 (A) CN-GM, (B)
 GM.

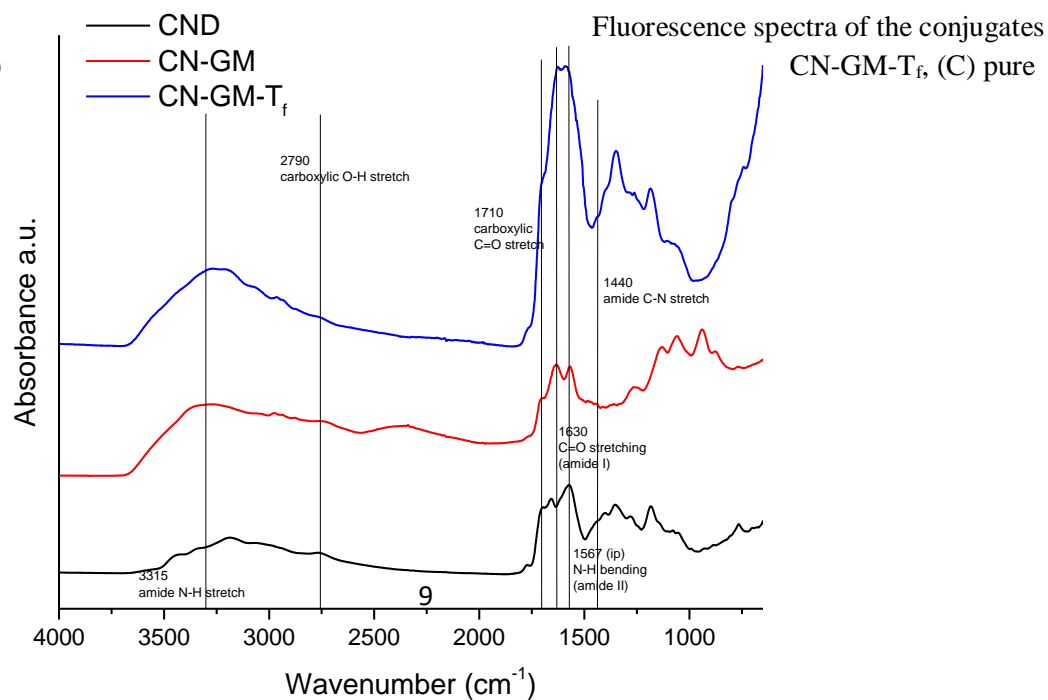


Fig. 3 ATR-FTIR spectra of the naked CNDs (black), CN-GM conjugate (red) and CN-GM-T_f conjugate (blue).

For further confirmation of successful conjugation, the conjugates were also characterized by MALDI-TOF spectrometry. As shown in Fig. 4A, the naked CNDs illustrated a molecular weight of 756 Da, which is consistent with our previous findings. In addition, CN-GM conjugate showed a molecular ion peak around 1512 Da. Considering the weight difference and that GM having a molecular weight of 263 Da, it can be hypothesized that roughly three molecules of GM are loaded on to one CND resulting in the molecular ratio of 1 : 3 for CND : GM in the conjugate produced. Fig. 4B shows the molecular ion peaks of pure T_f comparative to the CN-GM-T_f conjugate. As illustrated here, the molecular ion peaks for pure T_f and CN-GM-T_f are 80 454 and 85 907 Da, respectively. Thus, considering the same loading ratio above roughly three conjugate molecules of CN-GM were conjugated on to one T_f molecule in the formation of CN-GM-T_f, therefore, further increasing the GM loading capacity per molecule. These calculations also confirm the conjugation and the presence of all three initial compounds (CNDs, GM, T_f) in the synthesized conjugates and yields a final molecular ratio of 3 : 9 : 1 for CND : GM : T_f in the produced CN-GM-T_f conjugate resulting in a significantly higher GM drug loading ratio per carrier conjugate molecule.

Transmission electron microscopy (TEM) was conducted to obtain surface morphology images to determine the size distribution of the prepared conjugate nanomaterials in the X-Y plane. Prior to the measurements, the samples were sonicated for 5-10 min. to ensure the breakdown of any possible aggregate formations. In our previous work, the naked CNDs were found to have a narrow size distribution with a range of 1.0 – 3.8 nm and a mean diameter of 2.4 nm. Comparatively, as seen in figure 5A, the CN-GM conjugates are larger in size and have a size distribution of 3 – 6 nm. CN-GM-T_f conjugate dots are observed to be even larger in size with a diameter range of 8 – 12 nm (Fig. 5B). In addition, the shapes of the CN-GM-T_f conjugate seem to differ a bit from the original spherical shape found in both naked CNDs and CN-GM conjugate. This could be due to the interactions that occur in the presence of the protein; T_f.

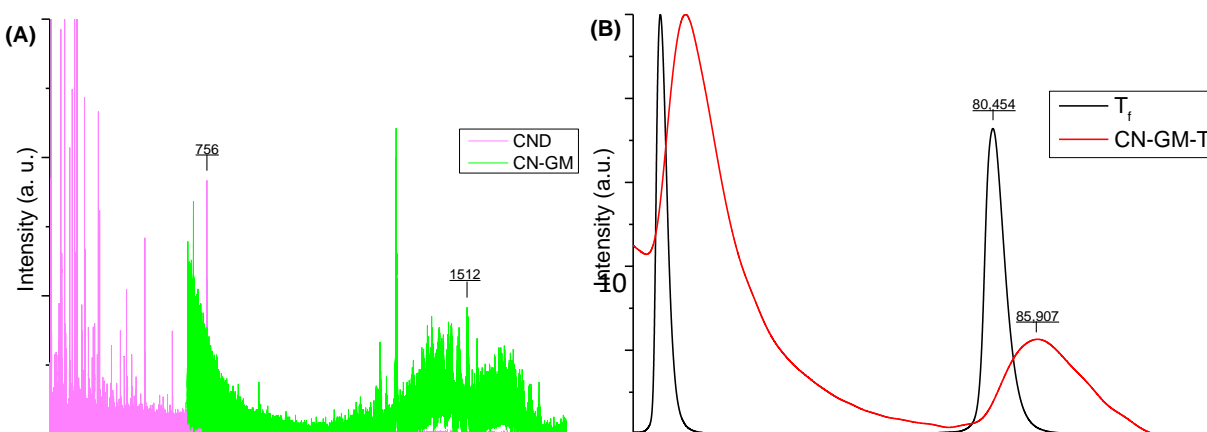


Fig. 4 MALDI-TOF mass spectra of (A) CNDs (purple), CN-GM conjugate (green), (B) T_f (black), CN-GM-T_f conjugate (red).

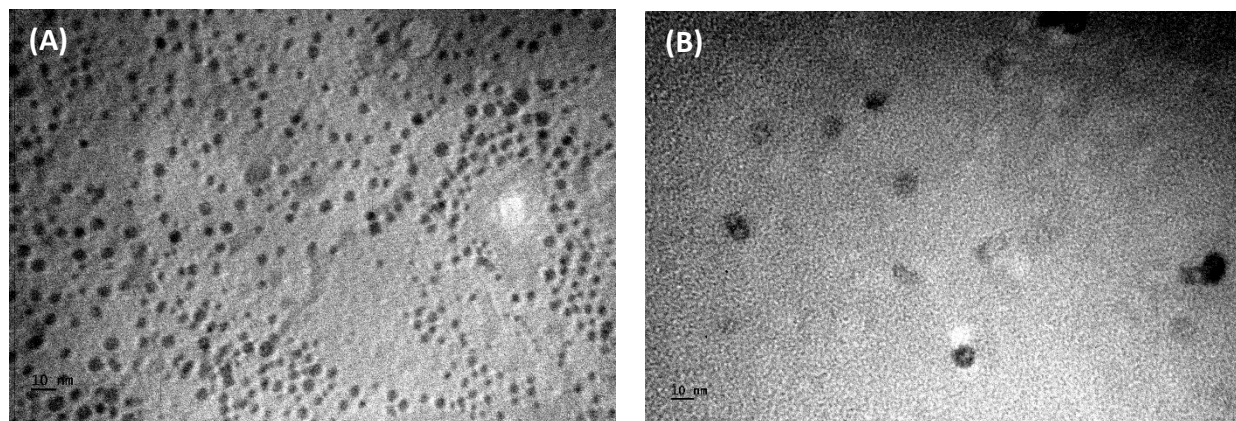


Fig. 5 TEM images of (A) CN-GM conjugate, (B) CN-GM-T_f conjugate.

According to our previous results on CNDs, we confirmed that these contain several types of functional groups on the surface such as -COOH, -CONH₂, -NH₂ and -OH using both FTIR and XPS data, due to which CNDs carry a negatively charged surface potential.⁴⁰ This large negative potential also allows the CNDs to be stable in water without rapid aggregation. For the conjugation discussed in this study, it is these -COOH groups that were used to form the peptide bonds with the amine groups present on the loading molecules, GM and T_f. Considering this, after the conjugation, the surface potential should differ from its original found on the naked CNDs. Therefore, surface Zeta potentials were measured for both conjugates in aqueous phase (Table 1). It is clearly noted that when GM is conjugated, the surface Zeta potential shows a drastic change compared to the original potential of CNDs. The decrease of the absolute value of potential could result from the reduction of the negatively charged -COOH functional groups due to conjugation. In contrast, CN-GM-T_f conjugate shows a much larger absolute value of surface potential which is quite closer to that of the naked CNDs compared to the CN-GM conjugate. Its potential was measured as -30.4 mV. The drastic change from CN-GM to CN-GM-T_f is due to the presence of the protein. Even though, as a result of the formation of the conjugate the CND loses some of the negatively charged functional groups, through the addition of T_f, which contains many negatively charged functionalities in its amino acid structure, the conjugate could regain a certain amount of negativity. Therefore, further conjugation to T_f shows a higher negative potential value compared to CN-GM. Further, dynamic light scattering (DLS) was conducted to measure size and dispersivity of the compounds. As shown in Table 1, the DLS size varies in the relation of CNDs < CN-GM < CN-GM-T_f. This increasing size confirms that the conjugate is forming adding each molecule to result in the larger conjugates. But, these size

measurements obtained are not reliable as the TEM data, due to the large hydrodynamic spheres that form around the highly functionalized nano-particle surface. Thus, the sphere tends to be larger than that of the actual CN or CN-conjugate, resulting in bulky measurements, although this confirms better dispersivity of the compounds even when the conjugates are formed, in the aqueous phase.

Table 1 Measured surface zeta potential for naked CNs and each conjugate.

Compound	Zeta Potential (mV)	DLS size (nm)
CNs	-38.8	139.3
CN-GM	-16.4	218.5
CN-GM-T _f	-30.4	322.6

Anticancer efficacy and glioma-cellular targeting

After confirming the presence of the conjugation and investigating the physicochemical properties, the as prepared conjugates were subjected to further *in vitro* studies to explore the anticancer efficacy and effectiveness. Through our previous studies on naked CNs we were able to confirm the selective targeting of CNs towards cancer cells. Therefore, first studies were carried out to determine the conjugates' capability for selective targeting. It is important to confirm that CNs do not lose this brain tumor selective targeting capability after going through the conjugation synthesis process. For this, we used SJGBM2 (high-grade pediatric glioma) and non-cancerous HEK293 (normal human embryonic kidney) cells as the cell specimens. Both SJGBM2 and HEK293 cell lines were treated with each of the conjugates, CN-GM and CN-GM-T_f at a concentration of 50 µg/ml. It is noteworthy to mention that all conjugates were able to disperse in the cell growth media (RPMI) owing to their excellent hydrophilic properties. The cells were incubated in the respective conjugate dispersed media for 24 h before fixing and mounting for imaging. A confocal microscope was used for the imaging conducted (Fig. 6 A,B,C). To not interfere with the auto fluorescence emitting from cell bodies in the blue region, the bioimaging was performed in longer wavelengths by exciting at 543 nm owing to the CNs' characteristic of excitation-dependent PL emission. As seen in Fig. 6, both CN-GM (Fig. 6A) and CN-GM-T_f (Fig. 6B) were capable of entering the cytoplasm of SJGBM2 cells. Some red colored patches can also be seen inside the cell nucleus which suggests that both conjugates are capable of reaching the nucleus. Furthermore, elaborating on the cell shapes and conditions after incubating with the conjugates, the cells seem deformed from their original shape. The cell nucleus also observed to be crippled and disfigured from its original large disc-shape. This also suggests that the conjugates are actively damaging the cancer cells. In contrast, the normal HEK293 cells do not show significant fluorescence when imaged (Fig. 6C), indicating that the conjugates are not actively entering the HEK293 cell bodies. A small quantity of conjugates can still cross the cellular membrane through passive diffusion owing to their still considerably small sizes, which yields a very weak fluorescence signal which can be considered negligible when compared to the fluorescence obtained from the SJGBM2 tumor cells. To confirm this

observation, fluorescence quantification analysis was conducted. The microscopy images were obtained using an inverted fluorescence microscope (Olympus BX51) at 20x and the cell fluorescence intensity was quantified using imageJ (captured images and the respective intensity distributions are shown in Fig. S3). For the CN-GM treatment, SJGBM2 cell line shows a mean fluorescence intensity of 38.386 ± 1.744 while the HEK293 only shows a mean intensity of 13.976 ± 1.098 (Fig. 6D). As shown in Fig. 6E, the two distributions show a significant difference in intensity, thus it can be confirmed that the CNDs preferentially enters SJGBM2 tumor cells while not significantly targeting non-cancerous HEK293 cells. Therefore, this further confirms our previous hypothesis of CNDs disguising as glutamine to selectively target cancerous cells as an essential metabolite and enter the cells through glutamine transporter, ASCT2. Moreover, according to previous studies, it has been found that some of these brain tumor cells overexpress glutamine transporters due to their high metabolic requirements.⁴⁴ T_f receptors have been found to be overexpressed in many cancer cells, specifically brain tumors due to the high iron demand.⁴⁵ Therefore, by loading T_f protein on to the nanocarrier, CN-GM- T_f was expected to have an increased cell uptake due to receptor-mediated endocytosis. But as shown in Fig. 6B and Fig. 6D, when treated with the CN-GM- T_f , the fluorescence intensity observed was lower than that of CN-GM rather than an increase. This could be resulting due to the decrease of CNDs PL by the large protein molecule present in the conjugate covering the small CNDs. Another possible reason is that due to the high molecular weight from the T_f , resulting in an extremely larger conjugate molecular weight the overall uptake could be lower, due to low molar concentrations. In comparison, this effect was not observed in the CN-GM- T_f treated HEK293 cell line, as observed in the intensity distribution in Fig. 6D. This result could be due to the high abundance of T_f receptors in the HEK293 cell line, thus uptaking high amounts through receptor mediated methods, regardless the low molar concentrations present. HEK293 is a kidney originated cell line, where T_f receptors are reported to be in abundance to encourage this uptake.⁴⁶

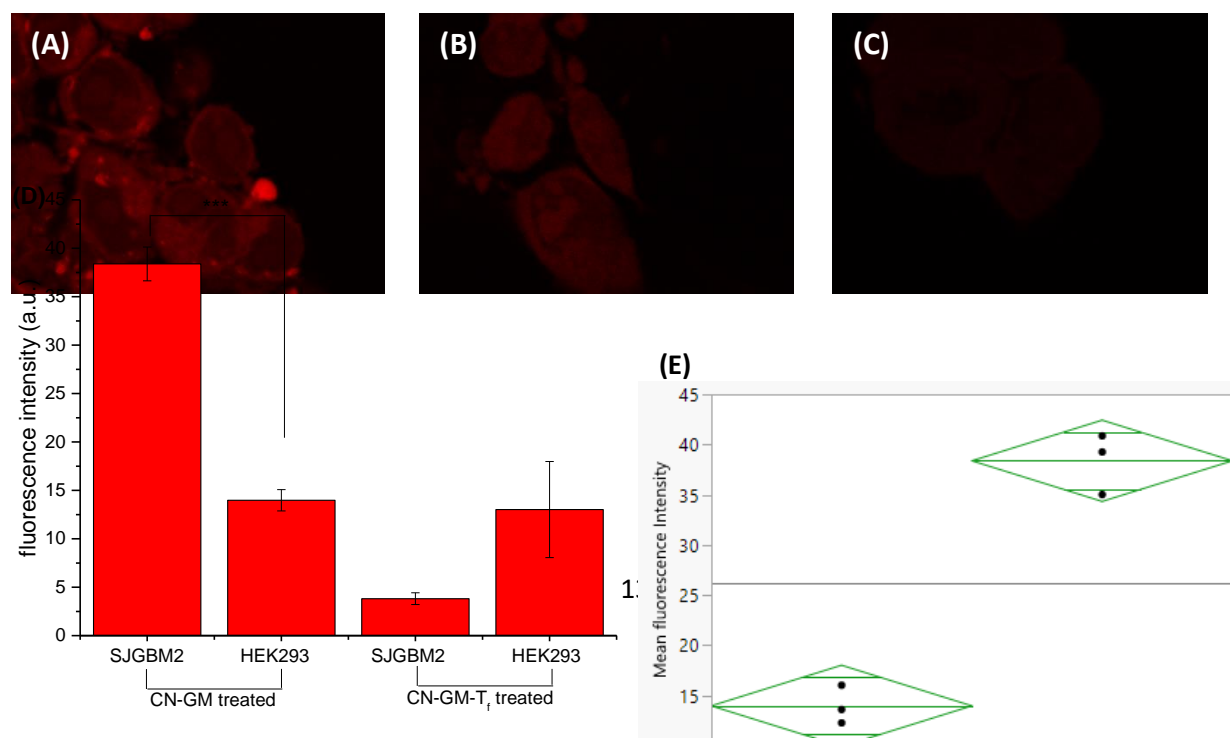


Fig. 6 Confocal images of both pediatric glioblastoma tumor and non-tumor cells after incubating with each conjugate at a concentration of 50 $\mu\text{g/ml}$ for 24 h. (A) SJGBM2 cells incubated in CN-GM conjugate, (B) SJGBM2 cells incubated in CN-GM- T_f conjugate, (C) HEK293 cells incubated in CN-GM conjugate. (Excitation at 543 nm). (D) Mean fluorescence intensity distribution obtained using inverted fluorescence microscope, for each cell type and treatment line. Standard errors included from 3 replicates. (E) One-way statistical analysis for the CN-GM treated two cell lines (SJGBM2, HEK293) at significance level $***p < 0.05$.

To investigate the efficacy of the as prepared conjugates on the tumor cells, *in vitro* viability studies were conducted. For these studies several types of pediatric brain tumor cell lines (SJGBM2, CHLA200, CHLA266) derived from patients at different times of treatments were used. Other than to the pediatric tumors, an adult glioblastoma cell line was also tested along with the non-cancerous HEK293 cell line. All cells were first plated and incubated for 24 h before being treated with the respective concentrations of GM, CN-GM or CN-GM- T_f conjugate RPMI media dispersions. After the treatment they were incubated for another 72 h before testing for viability. The viability studies were conducted using an MTS assay and the absorption measurements were recorded under the wavelength, 490 nm. The obtained averaged viability results after three repetitions are shown in Fig. 7 indicating the standard error. To determine the effect of single agent GM in brain tumor cell lines, we determined the IC₅₀ by treating the cells with increasing concentrations and determining viability 72 h later. The cell viability of different cell lines are shown when treated with CN-GM (Fig. 7A), and CN-GM- T_f (Fig. 7B). As seen in Fig. 7C, when treated with single agent GM, the best anti-cancer activity was observed on the GBM cell lines compared to the AT/RT cell line CHLA266. AT/RT is an aggressive pediatric brain tumor primarily affecting infants and toddlers with a dismal prognosis. These results confirm that GM is a possible new drug candidate for these aggressive brain tumors. Furthermore, at both 1, 0.1 μM concentrations, single agent GM were found to be cytotoxic towards the non-cancerous HEK293 cell line, showing a viability of $< 5\%$. Meanwhile, when treated with the CN-GM conjugate (Fig. 7A), it was found that the drug concentration was too high at 10 μM , that it killed all types of cells including the normal cells at a significant level. But, at a concentration of 1 μM , a drastic difference was observed where the SJGBM2 cell cytotoxicity level indicated to be $> 95\%$ while the HEK293 normal cell line was barely affected with an insignificant cytotoxicity as low as 2-3%, opposed to the single agent GM where it killed $> 95\%$ HEK293 cells at 1 μM . Therefore, the CN-GM conjugate was able to achieve the selective targeting of tumor cells without affecting the others. Another surprising discovery is that the U87 cell line showed a 60% cytotoxicity level when treated with the CN-GM conjugate whereas the single agent GM had no observable effect at 1 μM . Nonetheless, the selective anti-cancer efficacy of CN-GM conjugate was only limited to 1 μM and when treated at much lower quantities, its effect was drastically decreased. Therefore, as a possible technique to increase the

efficacy and to lower the effective drug dose, T_f was also attached in synthesis of CN-GM- T_f conjugate. It is widely known that brain tumor cells contain an abundant amount of T_f receptors because of their high iron demand. For the viability studies of CN-GM- T_f , the cell lines were treated with 100, 10 and 1 nM concentrations of the conjugate (Fig. 7B). At 1 μ M, it was observed that the concentration was too high and thus, the conjugate loses the selective targeting capability, causing apoptosis of the normal cells (data not shown). The non-selective cytotoxicity was still observable even at 100 nM of CN-GM- T_f . This effect could be arising due to the receptor-mediated endocytosis of T_f overcoming the selective targeting capability of CNDs at its high concentrations. HEK293 cells are derived from the kidney, which are also known to have high amounts of T_f receptors compared to other normal cells. Therefore, by binding T_f on to the nanocarrier, the nanocarrier entry to these cells increases drastically, through receptor-mediated endocytosis. Thus, this observed effect is reasonable. Hence, the treatment concentrations were further lowered to 10 and 1 nM. At 10 nM of CN-GM- T_f , a very similar result to that of CN-GM at 1 μ M was observed where the cytotoxicity on SJGBM2 was around 95% while it did not have any effect on the HEK293 cells. Furthermore, this low concentration (10 nM) still showed significant anti-cancer activity over other brain tumor cells. Thus, by attaching the T_f on the nanocarrier system, the concentration was lowered 100-fold while the same selective targeting and the anti-cancer activity preserved.

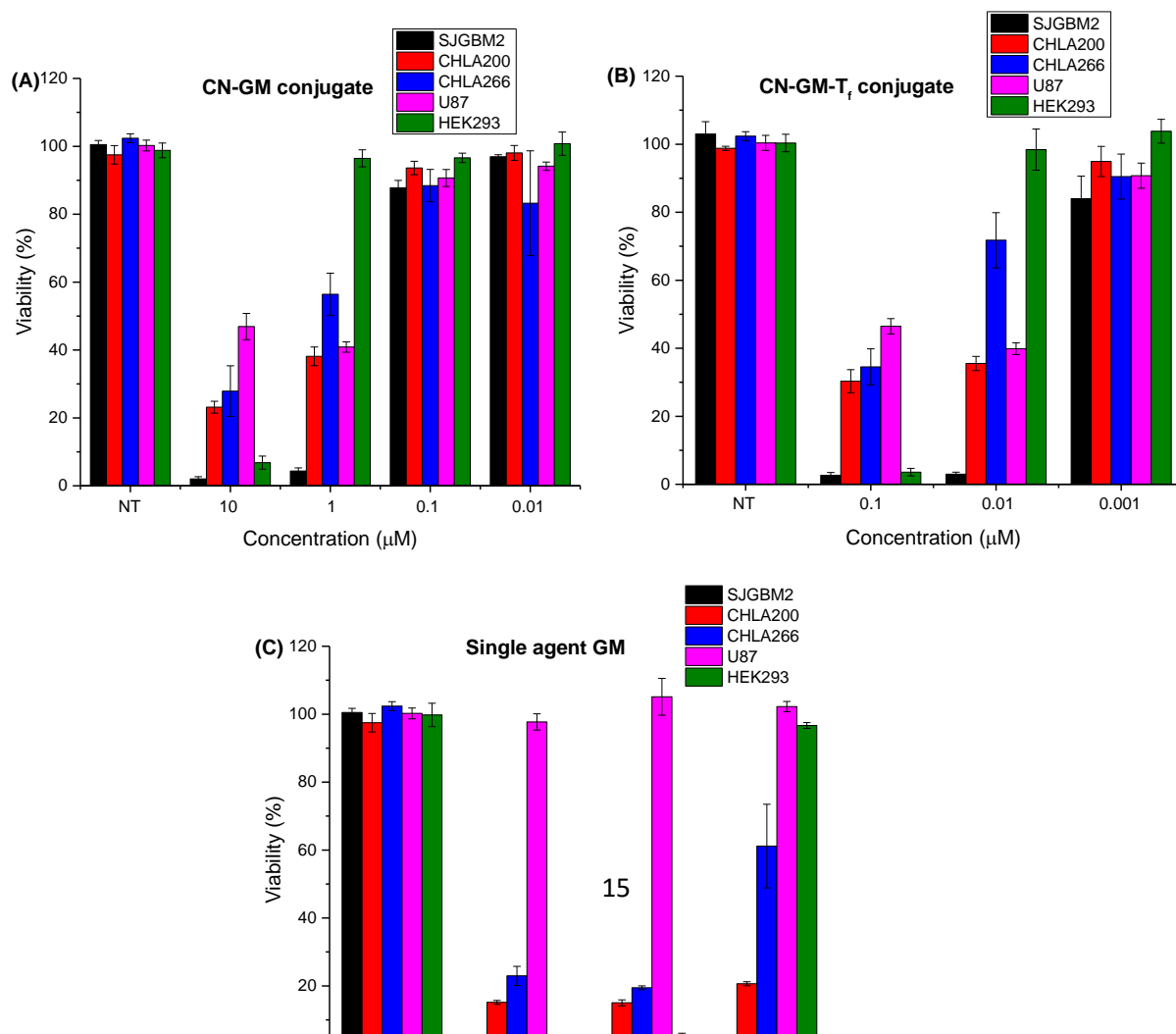


Fig. 7 *In vitro* viability studies to detect the effect of (A) CN-GM conjugate, (B) CN-GM-T_f conjugate and (C) single agent GM on different pediatric brain tumor cells and normal cells. Viability was determined after 72 h of incubation using an MTS assay. (NT – non-treatment).

BBB penetration

Then these conjugates were further examined for their capability to penetrate the BBB. It is important to investigate this ability, since the study is focused on targeted delivery into the brain. Many (> 95%) effective cancer drugs in the pharmacological industry are not capable of directly crossing the BBB to enter the CNS for the treatments, thus achieving this hurdle increases the carrier capability of the nano-dot. A zebrafish model was used for this investigation considering its' translucent body, rapid reproduction, ease of maintenance and genetic homology to humans. The CNS of zebrafish is connected by the cerebral spinal fluid. It circulates through ventricles of the brain which is contiguous with the central canal of spinal cord. Any fluorescent species that can penetrate the BBB will be observed in the spinal cord's central canal. Therefore, in our study, to test the ability of CNDs and CN-GM conjugate to overcome the BBB, the main assay is to observe if they can reach the central canal of spinal cord after intravascular heart injection.

To study if CNDs can pass the BBB, 10 mg/ml CNDs aqueous dispersion was intravascularly injected into the heart of wild-type zebrafish, which was repeated with 12 zebrafish to confirm the reproducibility of the results. Under the excitation of 405 nm, we observed the blue PL of the zebrafish vasculature in the CNDs channel. Also, in the location of central canal of spinal cord, blue PL was clearly observed, as pointed in Fig. 8. (Note: for convenience of display, blue PL was replaced by white color for better contrast against the dark background). This experiment shows the capability of naked CNDs to cross the BBB and a great potential for CNS-targeting drug delivery using CNDs as a nanocarrier. As for the mechanism of BBB penetration, we hypothesize that it is due to unique structural properties of CNDs as well as to its small size. It is well known that 99% of the molecules are not capable of crossing the BBB due to various restrictions BBB has to offer. The molecules can only cross the barrier via the active routes such as carrier-mediated transport by protein transporters (glucose, glutamate), receptor-mediated endocytosis (T_f receptor) or by passive diffusion.¹⁷ For a molecule to be able to penetrate the BBB by passive diffusion, the molecule should be significantly small and less hydrophilic. To be able to use a transporter-mediated channel, the molecules should either carry the relevant transporter molecules/ligands or mimic such molecules. In this stead, our hypothesis of the capability of CNDs to cross the BBB is due to its ability to mimic the structure of glutamine, thus using the ASCT2 transporter to cross the BBB. Furthermore, there is a possibility that a certain quantity of CNDs can cross the BBB through passive diffusion due to its small size.

So, as to confirm the capability of CNDs as an excellent nanocarrier for drug delivery targeting

the CNS, the previously obtained CN-GM conjugate (10 mg/ml) was intravascularly injected into the heart of 5 pdf wild-type zebrafish. To ensure the accuracy and reproducibility of the result, 12 zebrafish was applied to repeat the experiment. Under the excitation of 405 nm, we again observed the blue PL (replaced with white) in the vasculature and spinal cords' central canal (shown in the middle row of Fig. 8). Thus, the experiment shows that conjugation with GM did not affect the ability of CNDs to penetrate the BBB, which confirms that CNDs is an excellent drug nanocarrier targeting the CNS diseases, due to its self-ability of penetrating the BBB without an aid such as T_f . It has been previously reported that the BBB is overexpressed with T_f receptors to aid the iron demand in the brain⁴⁷ and by conjugating with T_f , the carbon nanoparticles are inevitably capable of crossing the BBB, in spite of their self-inability to cross.²⁴ Thus, considering the overexpression of T_f receptors on the BBB, conjugating with T_f can further increase the BBB penetration of the as prepared CN-GM- T_f nanocarrier conjugate.

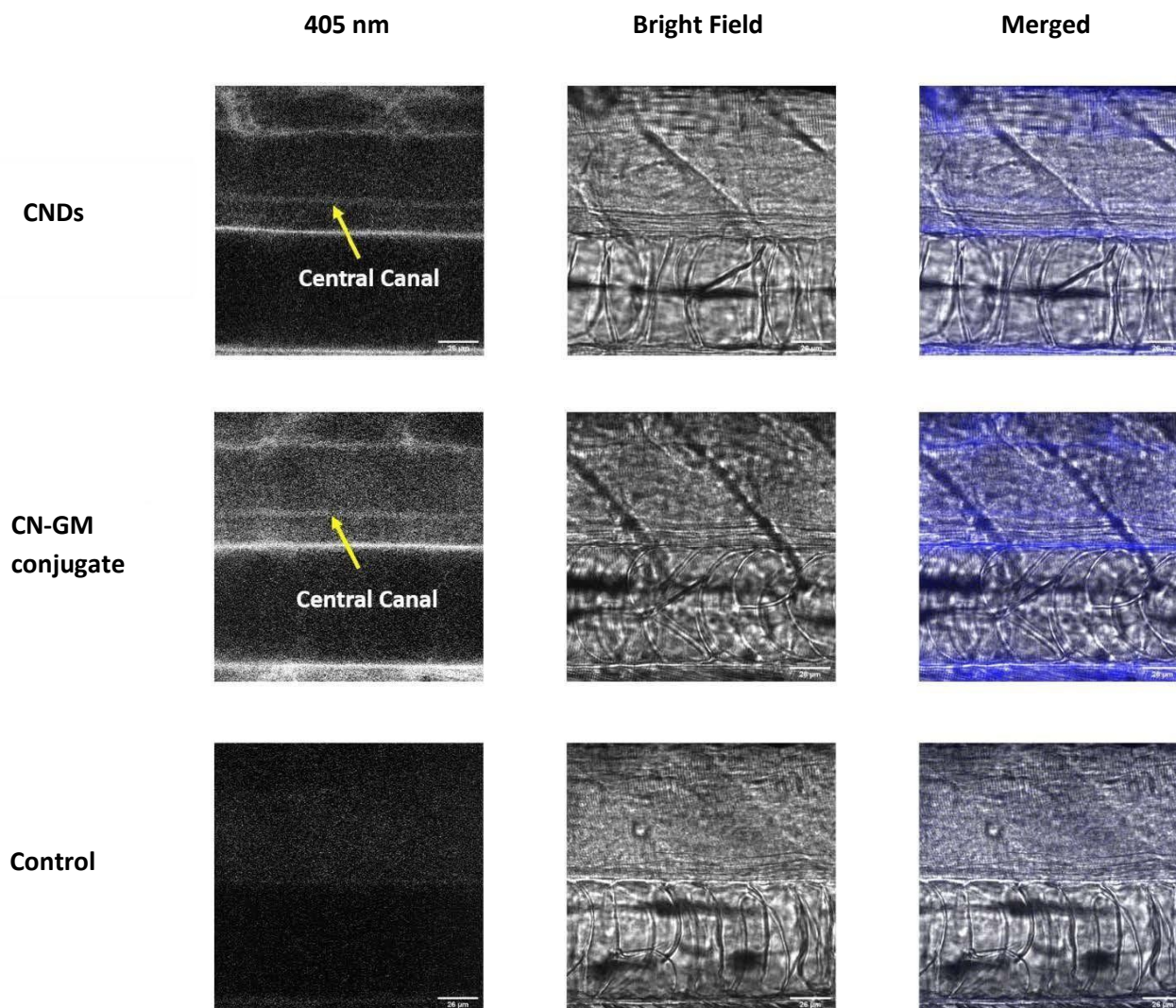


Fig. 8 Confocal microscopic images of five-day-old wild-type zebrafish larvae injected with 10 mg/ml naked CNDs aqueous dispersion (top row) and CN-GM conjugate aqueous dispersion (middle row). The lower row shows images of a fish without any injection as the control. Fluorescence from CNDs and CN-GM (405 nm excitation) that cross the BBB can be seen in the central canal (pointed with the yellow arrows).

4. Conclusion

In this study, a nanocarrier conjugation system was developed through the synthesis of two conjugates by effective loading of GM and T_f on to CNDs and extensively characterized after careful purification. Characterizations such as UV-Vis, luminescence, MALDI-TOF, FTIR spectroscopies, TEM and Zeta potential were utilized to confirm the success of the conjugation. Then, the conjugates were tested for their capability to selectively target the pediatric glioblastoma cells possibly utilizing the ASCT2 transporter channels by involving both *in vitro* cytotoxicity studies and bioimaging. Both conjugates were capable of targeting pediatric brain tumors while not affecting the normal cells at certain concentrations. At a high concentration as 1 μ M, the CN-GM conjugate was capable of targeting the tumor cells without affecting the normal cells, whereas the single agent GM showed extreme cytotoxicity towards normal cells. Importantly, when T_f is conjugated, the CN-GM- T_f conjugate was capable of specifically causing apoptosis of the GBM cells without affecting the HEK293 cells at a 100-fold lower concentration than when T_f is absent in the conjugate, although at higher concentrations it caused cell death of even the normal cells, possibly due to the cellular entry competition between the CNDs and T_f , which result in a higher cellular uptake. In addition, it was important to discover that both CNDs and CN-GM conjugate were capable of penetrating the BBB using a zebrafish model, which further confirms the potential of CNDs as a promising drug nanocarrier which can cross the BBB by itself and target tumors for the effective treatment of pediatric brain tumors. In summary, we were capable of constructing a conjugate system with a new glioma drug candidate, GM using CNDs as nanocarriers which offers the selective targeting of the cancerous cells as well as crossing BBB, thus overcoming both major obstacles present in pediatric glioblastoma chemotherapy treatments.

Declaration of competing interest

The authors declare no competing financial interest.

Acknowledgements

R.M.L. gratefully acknowledges the support of the National Science Foundation under grant 011298. Also, authors gratefully acknowledge the generous support from King Abdulaziz University, Kingdom of Saudi Arabia, and University of Miami, USA. R.M.G. gratefully acknowledges the support of the Mystic Force Foundation

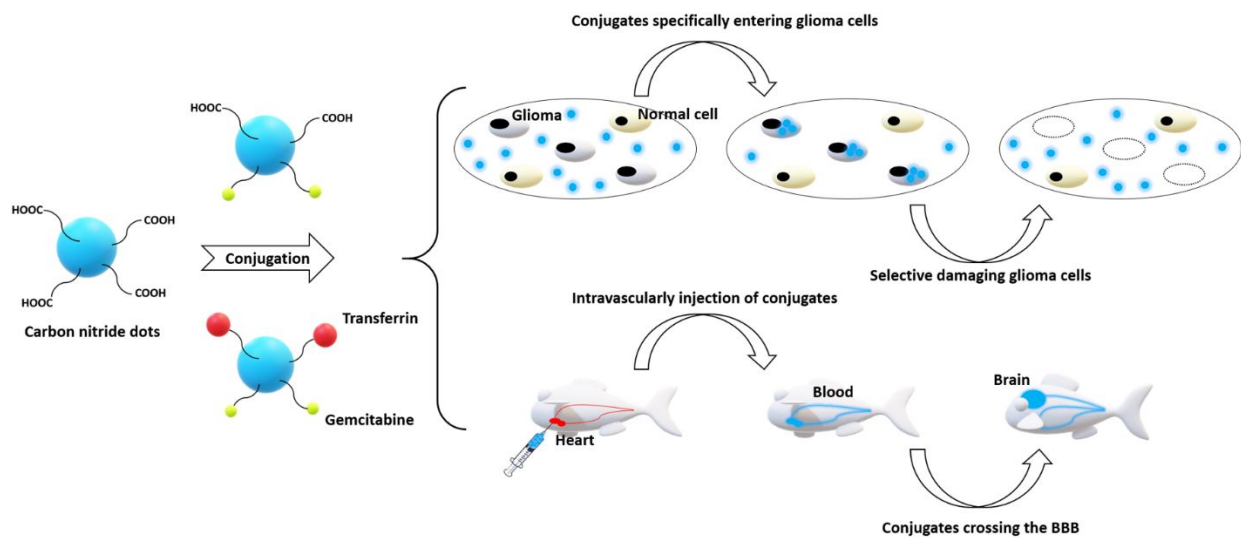
Supplementary Data

Supplementary data to this article can be found online.

References

- [1] D.N. Louis, H. Ohgaki, O.D. Wiestler, W.K. Cavenee, P.C. Burger, A. Jouvet, B.W. Scheithauer and P. Kleihues, *Acta Neuropathol.*, 2007, **114**, 97-109.
- [2] N.C. Institute, Adult central nervous system tumors treatment (PDQ®)—patient version, (2018).
- [3] Q.T. Ostrom, H. Gittleman, G. Truitt, A. Boscia, C. Kruchko and J.S. Barnholtz-Sloan, *Neuro-Oncol.*, 2018, **20**, iv1-iv86.
- [4] A. Korshunov, M. Ryzhova, V. Hovestadt, S. Bender, D. Sturm, D. Capper, J. Meyer, D. Schrimpf, M. Kool, P.A. Northcott, O. Zheludkova, T. Milde, O. Witt, A.E. Kulozik, G. Reifenberger, N. Jabado, A. Perry, P. Lichter, A. von Deimling, S.M. Pfister and D.T.W.J.A.N. Jones, *Acta Neuropathol.*, 2015, **129**, 669-678.
- [5] L. Bjerke, A. Mackay, M. Nandhabalan, A. Burford, A. Jury, S. Popov, D.A. Bax, D. Carvalho, K.R. Taylor, M. Vinci, I. Bajrami, I.M. McGonnell, C.J. Lord, R.M. Reis, D. Hargrave, A. Ashworth, P. Workman and C. Jones, *Cancer Discov.*, 2013, **3**, 512-519.
- [6] B.S. Paugh, A. Broniscer, C. Qu, C.P. Miller, J. Zhang, R.G. Tatevossian, J.M. Olson, J.R. Geyer, S.N. Chi, N.S. da Silva, A. Onar-Thomas, J.N. Baker, A. Gajjar, D.W. Ellison and S.J. Baker, *J. Clin. Oncol.*, 2011, **29**, 3999-4006.
- [7] C. Jones and S.J. Baker, *Nat. Rev. Cancer*, 2014, **14**, 651-661.
- [8] C. Jones, L. Perryman and D. Hargrave, *Nat. Rev. Clin. Oncol.*, 2012, **9**, 400-413.
- [9] S. Li, D. Amat, Z. Peng, S. Vanni, S. Raskin, G. De Angulo, A.M. Othman, R.M. Graham and R.M. Leblanc, *Nanoscale*, 2016, **8**, 16662-16669.
- [10] K.J. Cohen, I.F. Pollack, T. Zhou, A. Buxton, E.J. Holmes, P.C. Burger, D.J. Brat, M.K. Rosenblum, R.L. Hamilton, R.S. Lavey and R.L. Heideman, *Neuro-oncol.*, 2011, **13**, 317-323.
- [11] G.W. Robinson, B.A. Orr and A. Gajjar, *BMC Cancer*, 2014, **14**, 258.
- [12] S. Sengupta, J. Marrinan, C. Frishman and P. Sampath, *Clin. Dev. Immunol.*, 2012, **2012**, 831090.
- [13] M.A. Mityr and J.G. Edwards, *Int. J. Cardiol. Heart Vasc.*, 2016, **10**, 17-24.
- [14] N. Marina, *Pediatr. Clin. N. Am.*, 1997, **44**, 1021-1042.
- [15] D.A. Mulrooney, M.W. Yeazel, T. Kawashima, A.C. Mertens, P. Mitby, M. Stovall, S.S. Donaldson, D.M. Green, C.A. Sklar, L.L. Robison and W.M. Leisenring, *BMJ*, 2009, **339**, b4606.
- [16] M. Tukenova, C. Guibout, O. Oberlin, F. Doyon, A. Mousannif, N. Haddy, S. Guérin, H. Pacquement, A. Aouba, M. Hawkins, D. Winter, J. Bourhis, D. Lefkopoulos, I. Diallo and F. de Vathaire, *J. Clin. Oncol.*, 2010, **28**, 1308-1315.
- [17] Y. Zhou, Z. Peng, E.S. Seven and R.M. Leblanc, *J. Control. Release*, 2018, **270**, 290-303.
- [18] I. Zeiadeh, A. Najjar and R. Karaman, *Molecules*, 2018, **23**, 1289.
- [19] H.S. Sharma and A. Sharma, H.S. Sharma (Ed.) Progress in Brain Research, *Elsevier*, 2007, 245-273.
- [20] S.-K. Wu, P.-C. Chu, W.-Y. Chai, S.-T. Kang, C.-H. Tsai, C.-H. Fan, C.-K. Yeh and H.-L. Liu, *Sci. Rep.*, 2017, **7**, 46689.
- [21] P.-C. Chu, W.-Y. Chai, C.-H. Tsai, S.-T. Kang, C.-K. Yeh and H.-L. Liu, *Sci. Rep.*, 2016, **6**, 33264.
- [22] X. Gao and C. Li, *Small*, 2014, **10**, 426-440.
- [23] S. Lu, S. Guo, P. Xu, X. Li, Y. Zhao, W. Gu and M. Xue, *Int. J. Nanomed.*, 2016, **11**, 6325-6336.
- [24] S. Li, Z. Peng, J. Dallman, J. Baker, A.M. Othman, P.L. Blackwelder and R.M. Leblanc, *Colloids Surf. B Biointerfaces*, 2016, **145**, 251-256.
- [25] Z.M. Qian, H. Li, H. Sun and K. Ho, *Pharmacol. Rev.*, 2002, **54**, 561-587.
- [26] Z.C. Soe, J.B. Kwon, R.K. Thapa, W. Ou, H.T. Nguyen, M. Gautam, K.T. Oh, H.-G. Choi, S.K. Ku, C.S. Yong and J.O. Kim, *Pharmaceutics*, 2019, **11**, 63.
- [27] O. Grinberg, A. Gedanken, C.R. Patra, S. Patra, P. Mukherjee and D. Mukhopadhyay, *Acta Biomater.*, 2009, **5**, 3031-3037.

- [28] H. Hosseinzadeh, F. Atyabi, R. Dinarvand and S.N. Ostad, *Int. J. Nanomed.*, 2012, **7**, 1851-1863.
- [29] S.Z. Gertler, D. MacDonald, M. Goodyear, P. Forsyth, D.J. Stewart, K. Belanger, J. Perry, D. Fulton, W. Steward, N. Wainman and L. Seymour, *Ann. Oncol.*, 2000, **11**, 315-318.
- [30] M. Weller, J. Streffer, W. Wick, R.D. Kortmann, E. Heiss, W. Küker, R. Meyermann, J. Dichgans and M. Bamberg, *Cancer*, 2001, **91**, 423-427.
- [31] W. Wick, M. Hermisson, R.D. Kortmann, W.M. Küker, F. Duffner, J. Dichgans, M. Bamberg and M. Weller, *J. Neuro-Oncol.*, 2002, **59**, 151-155.
- [32] S.E.M. Veldhuijzen van Zanten, F.E. El-Khouly, M.H.A. Jansen, D.P. Bakker, E. Sanchez Aliaga, C.J.A. Haasbeek, N.I. Wolf, C.M. Zwaan, W.P. Vandertop, D.G. van Vuurden and G.J.L. Kaspers, *J. Neuro-Oncol.*, 2017, **135**, 307-315.
- [33] C. Bastiancich, G. Bastiat and F. Lagarce, *Drug Discov. Today*, 2018, **23**, 416-423.
- [34] J.Z. Kerr, S.L. Berg, R. Dauser, J. Nuchtern, M.J. Egorin, L. McGuffey, A. Aleksic and S. Blaney, *Cancer Chemother. Pharmacol.*, 2001, **47**, 411-414.
- [35] W. Wang, Y.-C. Lu, H. Huang, J.-J. Feng, J.-R. Chen and A.-J. Wang, *Analyst*, 2014, **139**, 1692-1696.
- [36] J. Zhou, Y. Yang and C.-y. Zhang, *Chem. Comm.*, 2013, **49**, 8605-8607.
- [37] J. Ma, B. Guo, X. Cao, Y. Lin, B. Yao, F. Li, W. Weng and L. Huang, *Talanta*, 2015, **143**, 205-211.
- [38] Z. Song, T. Lin, L. Lin, S. Lin, F. Fu, X. Wang and L. Guo, *Angew. Chem. Int. Ed.*, 2016, **55**, 2773-2777.
- [39] Y. Li, Y. Zhao, H. Cheng, Y. Hu, G. Shi, L. Dai and L. Qu, *J. Am. Chem. Soc.*, 2012, **134**, 15-18.
- [40] P.Y. Liyanage, R.M. Graham, R.R. Pandey, C.C. Chusuei, K.J. Mintz, Y. Zhou, J.K. Harper, W. Wu, A.H. Wikramanayake, S. Vanni and R.M. Leblanc, *Bioconjugate Chem.*, 2019, **30**, 111-123.
- [41] G.E. LeCroy, F. Messina, A. Sciortino, C.E. Bunker, P. Wang, K.A.S. Fernando and Y.-P. Sun, *J. Phys. Chem. C*, 2017, **121**, 28180-28186.
- [42] B. van Dam, H. Nie, B. Ju, E. Marino, J.M.J. Paulusse, P. Schall, M. Li and K. Dohnalová, *Small*, 2017, **13**, 1770251.
- [43] M.R. Alexander, S. Payan and T.M. Duc, *Surf. Interface Anal.*, 1998, **26**, 961-973.
- [44] M. Dolińska, A. Dybel, B. Zabłocka and J. Albrecht, *Neurochem. Int.*, 2003, **43**, 501-507.
- [45] S. Dixit, T. Novak, K. Miller, Y. Zhu, M.E. Kenney and A.-M. Broome, *Nanoscale*, 2015, **7**, 1782-1790.
- [46] D. Zhang, E. Meyron-Holtz and T.A. Rouault, *J. Am. Soc. Nephrol.*, 2007, **18**, 401-406.
- [47] T. Moos and E.H. Morgan, *Cell. Mol. Neurobiol.*, 2000, **20**, 77-95.



Graphical Abstract